CONF-850871--8

HIGH-ENERGY NEUTRON SPECTROSCOPY ON f-ELECTRON OXIDES

S. Kern
Physics Dept., Colorado State University,
Fort Collins, Colorado, 80523 USA

CONF-850871--8
DE85 017387

C.-K. Loong and G.H. Lander
Intense Pulsed Neutron Source,
Argonne National Laboratory, Argonne, Illinois, 60439 USA

Abstract

Neutron inelastic scattering with the chopper spectrometers at IPNS has been used to measure, for the first time, the ground to excited crystal-field transitions in PrO_2 (130 meV), $BaPrO_3$ (255 meV), and UO_2 ($\sim$ 160 meV). From these measurements we deduce the values of $V_4 = A_4 \langle r^4 \rangle$ and compare both the absolute values and their variation with theoretical estimates. In the case of UO_2 two peaks are seen, one at 155 and the other at 172 meV. This structure exists both below and above T_N (30.8K) and we believe is caused by a dynamic Jahn-Teller effect that splits the excited Γ_3 state.

International Conference of Neutron Scattering, Aug. 19-23, 1985, Santa Fe, New Mexico, USA
To be published in Physica

Introduction

Neutron spectroscopy provides the most direct method of determining crystal-field (cf) potentials in materials. Scattering from the vibrational modes of the lattice can be separated from magnetic scattering by the different dependence of the two types of scattering on the momentum transfer Q. An even more precise separation may be performed if sufficient neutron intensity is available to permit the use of polarization analysis. In contrast, optical techniques are frequently unable to separate electronic and vibronic contributions, and are less effective if the samples are opaque or if the cation resides at an inversion center, but have the advantage in intensity and resolution available. Furthermore, neutron spectroscopy of magnetic transition conventionally is limited to excitations $\lesssim$ 50 meV. Fortunately, cf splittings in metallic systems are indeed usually in this range, so neutrons have played a major role [1].

The lanthanide and actinide oxides have been extensively studied, [2,3] but the magnitudes of the potentials are still unknown.

Experimental Details

All experiments have been performed on the high resolution, medium energy, chopper spectrometer (HRMECS) at the Intense Pulsed Neutron Source (IPNS) at Argonne National Laboratory. A phased Fermi chopper produces pulses of monochromatic neutrons which are incident on the sample. The energy and momentum transfers are determined by neutron time-of-flight techniques in over 150 detectors. The energy resolution, $\delta E/E_o$, in general depends on the chopper in use and varies with energy transfer but is approximately 3-4%. Incident energies of 350, 500, and 800 meV have been used for these experiments.

The samples were prepared by standard methods, examined by x-rays to measure the lattice parameters [for PrO_2 a (cubic) = 5.392 Å, for $BaPrO_3$ the structure is orthorhombic a = 6.181, b = 6.214, c = 8.722 Å, for UO_2 a (cubic) = 5.470 Å] and search for additional phases, which were not found. In each case 100 - 120 g. of polycrystalline material was contained in a flat plate sample can and this holder was mounted on the cold plate of a DISPLEX refrigerator. The neutron beam (of dimensions 7.5 x 10.0 cm^2) was perpendicular to the plate so that for low angles the beam did not traverse more than 1 cm of material. Such a geometry minimizes multiple scattering of the neutrons. Samples of the nonmagnetic analogues CeO_2, $BaCeO_3$ and ThO_2 were also examined, but no crystal-field excitations were seen.

The data for PrO_2 have been presented previously [4]. A single peak is seen at 130 ± 5 meV with a width of ∿ 15 meV. The results for $BaPrO_3$ are shown in Fig. 1. The transition here is at 255 ± 10 meV, with a width of ∿ 25 meV, which is the instrumental resolution with E_o = 800 meV. The three spectra in Fig. 2 show that the peak intensity decreases with increasing scattering angle ϕ. This is because of form factor effects, and is expected.

The data for UO_2 are shown in Fig. 2 as a function of temperature. Two peaks are seen, particularly at low temperature, with a splitting between them of 17 ± 2 meV. At low temperature the peaks are at 155 ± 1 meV and 172 ± 2 meV. The widths of the peaks is ∿ 11 meV, which is essentially the expected resolution (∿ 10 meV) with E_o = 350 meV.

Results and Discussion

Details of the cf transition and parameters deduced from these measurements are given in Table 1. To specify the cf potential completely for an ion in a cubic or octahedral environment requires the two parameters V_4 and V_6. Since we have observed only one peak, we cannot determine two parameters.

However, we make the reasonable assumption that $V_6/V_4 \lesssim 0.05$, and can then determine V_4. These calculations are performed in intermediate coupling with well-established spin-orbit parameters.

For a cubic configuration and assuming the point-charge model, neglecting higher-order terms,

$$V_4 = A_4 \langle r^4 \rangle = - \frac{7}{18} \frac{Ze^2}{R^5} \langle r^4 \rangle \qquad (1)$$

For an octahedral configuration the (- 7/18) becomes (+ 7/16). Ze is the effective charge at the ligand, R is the cation-ligand separation, and $\langle r^n \rangle$ is the expectation value of the f electron distribution. Thus we can calculate the parameter (Ze^2) and this is given in Table 1. If the simple point charge model applied all the numbers should be the same. The model does predict the correct sign of V_4 but is otherwise inadequate.

In comparing $V_4(PrO_2)/V_4(BaPrO_3)$ the agreement can be much improved by increasing the dependence on R from the fifth to about the tenth power. This is consistent with current models [5].

In the case of UO_2 the value of the cf splitting is consistent with the predictions of Rahman and Runciman [6]. The scaling between UO_2 and PrO_2 for (Ze^2) is about a factor of two, consistent with the much stronger interaction between the expanded 5f electrons and the surrounding ions compared to the 4f electrons.

Of major importance is the discovery of a double peak structure in the UO_2 spectrum. Although calculations with the Russell-Saunders state lead to a Γ_4 close by the first excited Γ_3, intermediate-coupling calculations force the Γ_4 well above $\sim$ 400 meV. Indeed, with incident neutron energies of 800 meV we have seen no further transition up to $\sim$ 350 meV in UO_2. The figure shows that the two peaks are present at all temperatures up to at least 150 K and that both peaks decrease in energy a small amount ($\sim$ 5%) on warming from 10 to 150 K. In a separate experiment we have measured the response out to $Q \gtrsim 19$ $\mathring{A}^{-1}$ and shown unambiguously that both transitions are magnetic in origin.

Uranium dioxide orders antiferromagnetically [7,8] at 30.8 K. Spin-wave measurements [7] show that the exchange splitting of the ground state Γ_5 triplet is $\sim$ 13 meV and this may be the origin of the abrupt change in energy between 47 and 27 K. An internal rearrangement of the oxygen sub-lattice [8] is also observed in UO_2, and this gives rise to a quadrupole term that splits the Γ_3 doublet (this doublet is not split by the exchange magnetic field). However, calculations of such a static term give a splitting of the Γ_3 of $\sim$ 2 meV, much smaller than that observed. Despite this lack of agreement we believe that a dynamical splitting of the excited Γ_3 doublet is the reason for the two-peak structure in Fig. 2. For example, Sasaki and Obata [9] have shown that such a dynamical Jahn-Teller effect has a pronounced effect on both the susceptibility and the temperature dependence of the elastic constants [10], in which anomalies extend to $\sim$ 200 K despite the phase transition being at 30.8 K.

This work was supported by the U.S. Dept. of Energy, Basic Energy Sciences, Div. of Materials Science.

Keywords crystal-fields
oxides
actinides
pulsed sources

References

1. See, for example, "Crystalline Electric Field Effects in f Electron Magnetism", ed. R.P. Guertin, W. Suski, and Z. Zolnierek, Plenum Press, N.Y., (1982).
2. "Handbook on the Physics and Chemistry of Rare-Earths", ed. K. Gschneider and L. Eyring, North-Holland, Amsterdam, 1979. See Chapters 27 and 28.
3. J. Schoenes in "Handbook of the Physics and Chemistry of the Actinides", ed. A.J. Freeman and G.H. Lander, North-Holland, Amsterdam, 1984, Vol. 1, 341.
4. S. Kern, C.-K. Loong, J. Faber and G.H. Lander, Solid State Comm. 49, 295 (1984).
5. D.J. Newman, Adv. in Phys. 20, 197 (1971); M. Tovar, C.A. Ramos, and C. Fainstein, Phys. Rev. B28, 4813 (1983).
6. H.U. Rahman and W.A. Runciman, J. Phys. Chem. Solids 27, 1833 (1966).
7. R.A. Cowley and G. Dolling, Phys. Rev. 167, 464 (1968).
8. J. Faber and G.H. Lander, Phys. Rev. B14, 1151 (1976).
9. K. Sasaki and Y. Obata, J. Phys. Soc. Japan 28, 1157 (1970).
10. O.G. Brandt and C.T. Walker, Phys. Rev. 170, 528 (1968).

Figure Captions

Figure 1 Spectra for $BaPrO_3$ showing the $\Gamma_7 - \Gamma_8$ splitting. The inset shows the octahedral coordination of the Pr ion. The frames of data at different ϕ have Q = 3.9, 4.7 and 5.6 $\AA^{-1}$ from top to botton, respectively, and show the decrease of intensity as expected from the magnetic form fact .

Figure 2 Spectra for UO_2 as a function of temperature. The Q value at an energy transfer of 160 meV is 4.4 $\AA^{-1}$.

Table 1 Properties of three oxides as discussed in the text.

	PrO_2	$BaPrO_3$	UO_2
nearest neighbour environment	cubic	octa-hedral	cubic
no. f electron	$4f^1$	$4f^1$	$5f^2$
RS ground state manifold	$^2F_{5/2}$	$^2F_{5/2}$	$^3H_4$
energy to next J manifold (meV)	$\sim$ 370	$\sim$ 370	$\sim$ 500
crystal-field ground state	Γ_8	Γ_7	Γ_5
1st excited cf state	Γ_7	Γ_8	Γ_3
transition observed (meV)	130±5	255±10	155±1 172±2
V_4 (meV)	-(66±3)	+(119±4)	-(385±10)
V_6/V_4 (assumed)	0.05	0.05	0.05
R (Å)	2.335	2.225	2.369
$\langle r^4 \rangle$ a.u.	2.18	2.18	7.63
$(Ze^2) \langle r^4 \rangle \times 10^{-4}$ (meV-Å)	6.9 ±0.3	8.6 ±0.3	12.3 ±0.3

Fig 1

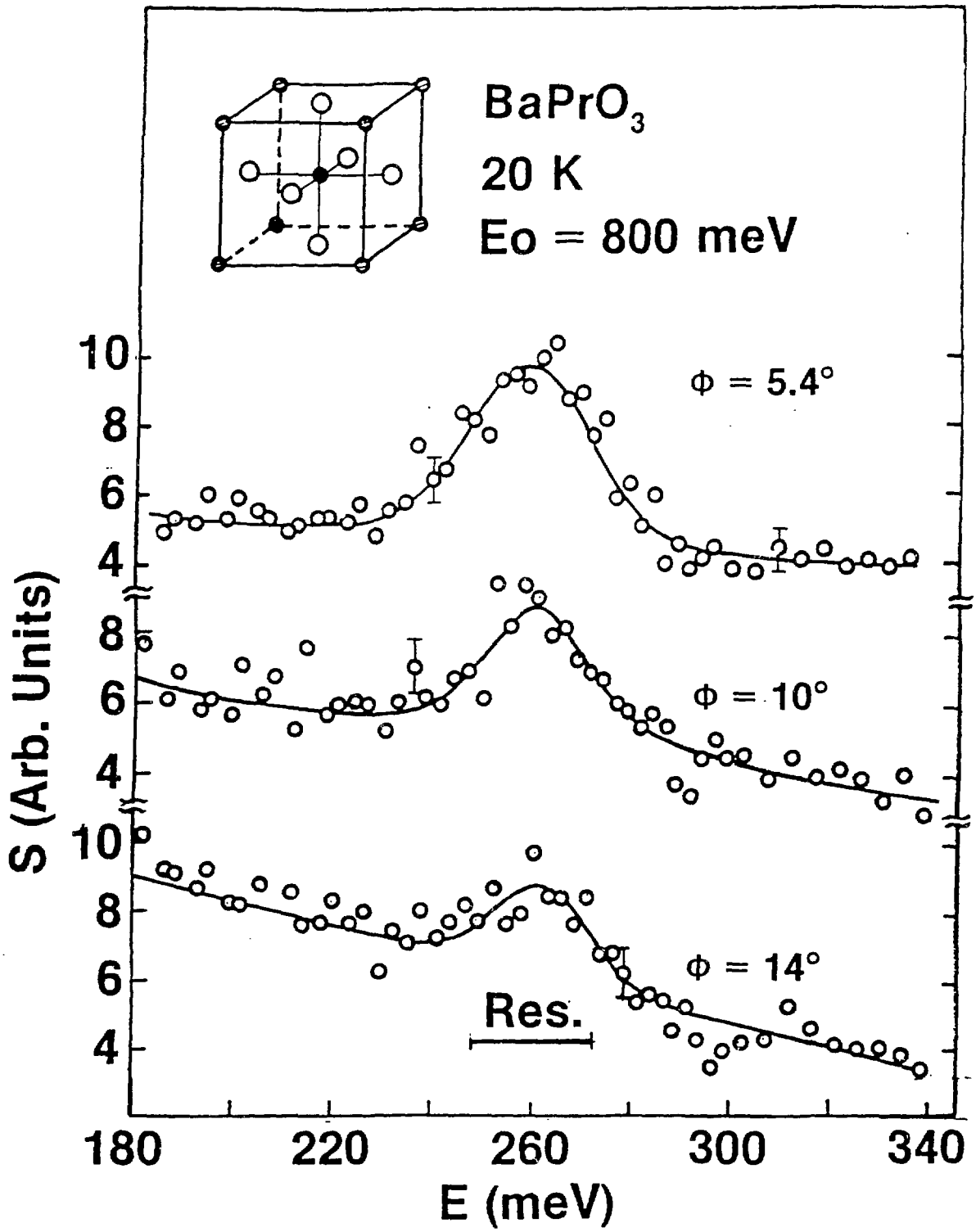
BaPrO3
20 K
Eo = 800 meV
Φ = 5.4°
Φ = 10°
Φ = 14°
Res.
S (Arb. Units)
E (meV)
180
220
260
300
340
10
8
6
4

Fig 2

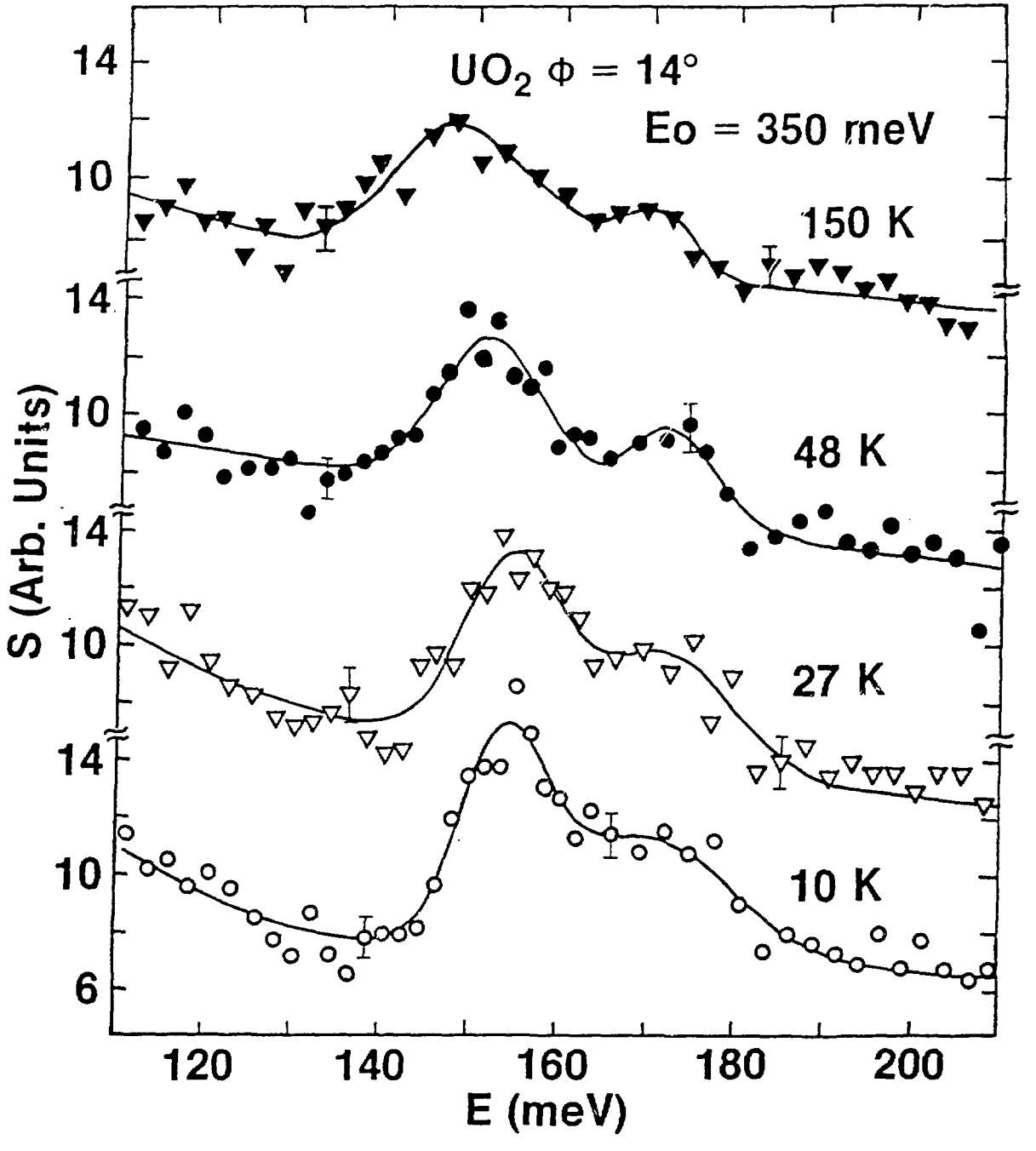
UO_2 Φ = 14°
Eo = 350 meV
150 K
48 K
27 K
10 K
S (Arb. Units)
E (meV)
14
10
14
10
14
10
14
10
6
120
140
160
180
200